Asian Journal of Chemistry; Vol. 32, No. 9 (2020), 2173-2179

ASIAN JOURNAL OF CHEMISTRY

https://doi.org/10.14233/ajchem.2020.22728

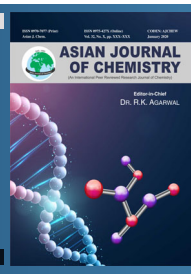

Enhancement Effect of Fe-Co-Ni/BC Nanoparticles for Membraneless Fuel Cells

V. SELVARANI[1], S. KIRUTHIKA[2], V. SUDHA[1], A. GAYATHRI[1] and B. MUTHUKUMARAN[1,*]

[1]Department of Chemistry, Presidency College (Autonomous), University of Madras, Chennai-600 005, India
[2]Department of Chemical Engineering, SRM Institute of Science and Technology, Chennai-603 203, India

*Corresponding author: Fax: +91 44 28510732; Tel: +91 44 28544894; E-mail: dr.muthukumaran@yahoo.com

Received: 19 March 2020; *Accepted*: 25 May 2020; *Published online*: 20 August 2020; AJC-20009

Biocarbon (BC) supported iron–cobalt–nickel (Fe–Co–Ni/BC) nanoalloy catalysts were synthesized by ultrasonic-assisted chemical reduction method. The morphological and physico-chemical characteristics show that the 1:1:1 composition of Fe–Co–Ni/BC catalyst has the Fe face-centered cubic (fcc) solid-solution structure showing the incorporation of Co and Ni. The electrocatalytic execution of this iron-based nanoalloy catalyst and its interaction with biocarbon was explored in a membraneless fuel cell and compared with carbon supported Fe–Co–Ni catalyst (Fe–Co–Ni/C). In a single-cell test, the power density obtained for Fe–Co–Ni/BC (35.4 mW/cm^2) was better than that of Fe–Co–Ni/C (31.3 mW/cm^2), utilizing 0.1 mol/L sodium perborate as oxidant and 1 mol/L ethylene glycol as fuel in an alkaline medium. The electrochemical findings revealed that the execution and solidness of the Fe–Co–Ni/BC catalyst is good and prevalent to that of Fe–Co–Ni/C catalyst. The better execution of BC-supported catalyst is due to its high electrical conductivity, high porosity and expansive surface area. It is been concluded that both the advantageous impact and the nature of support have an imperative part on the execution of Fe–Co–Ni/BC nanoalloy catalysts for the CO_2-free ethylene glycol oxidation. Subsequently, it is accepted that the BC-supported Fe–Co–Ni nanoalloy catalysts are anticipated to be broadly utilized in electrocatalytic energy-conversion applications.

Keywords: Membraneless fuel cell, Perborate, Ethylene glycol, Biocarbon, Nanoalloy.

INTRODUCTION

Nanocatalysts lead to key changes in energy storage and conversion. Statistical analysis of the present study on evaluation of non-precious metal catalysts with suitable support materials for electrochemical applications is still significant challenge. The effect of fossil fuel-based power generation has abruptly increased the atmospheric carbon dioxide levels. Consequently, it stimulates an exceptional energy drive towards cleaner sources of energy. There now exists a number of method in which the work can be extended and improved to develop energy-conversion applications. Fuel cell technology is still a developing technology that continuously converts the chemical energy into electricity both in the absence and presence of membrane by the direct oxidation-reduction reactions. At present, maximum sensible catalysts are platinum based catalysts for the higher catalytic activity in low temperature fuel cells. Due to its global scarcity, high costs and poor stability, recently, a high level of activity and stability is identified in iron-based catalysts, which are a promising successor for Pt-based catalysts. This was based on more resistant to attrition and much stronger than commercial Pt/C catalysts [1-5].

Catalysts are generally assisted on permeable and porous membranes in low temperature fuel cells [6]. It is evidenced that the supported metal catalysts have enhanced stability and higher area, porosity, electrical conductivity, electrochemical stability and functional surface groups characterize the support [7]. In like manner, numerous sorts of carbonaceous materials are examined as electrocatalyst supporters [8,9]. For occurrence, broad reports cover carbon blacks (Vulcan XC-72R), mesoporous carbons and nanostructured carbons with amazing come about [10]. As of late, the foremost one of the widely-used carbon support is biocarbon (BC). Because of its surface zone and high-quality digital conductivity, it has been preparing many fuel cell catalysts [11-14]. However, only limited research has been conducted in promoting biocarbon and carbon based supports for such applications.

In this consider, Fe-Co-Ni/BC and Fe-Co-Ni/C catalysts were synthesized through ultrasonic-assisted chemical reduction method from their precursors to study ethylene glycol

electro-oxidation. The prepared nanocatalysts were characterized utilizing TEM, EDX and XRD examinations. Ethylene glycol electrooxidation in presence of above catalysts was examined by utilizing CO-stripping voltammetry, cyclic voltametry (CV) and chronoamperometry (CA). At lengthy last, the catalyst was tried as anode in a microfluidic membraneless fuel cell.

EXPERIMENTAL

Cobalt(II) acetate tetrahydrate ($(CH_3COO)_2Co{\cdot}4H_2O$) (Merck), Iron(II) acetate ($Fe(C_2H_3O_2)_2$) (Sigma-Aldrich) and nickel(II) acetate tetrahydrate ($Ni(CH_3CO_2)_2{\cdot}4H_2O$) (Sigma-Aldrich) were metal antecedents utilized in this study for the preparation of electrocatalysts. Carbon (Sigma-Aldrich) and the biocarbon from coconut shell were utilized as support for the catalysts. Isopropanol (Merck)/water solution (50/50, v/v) were utilized as a solvent and sodium borohydride ($NaBH_4$) (Merck) were utilized as a reduction agent. The catalyst ink was made by Nafion® (DuPont USA, DE 521) dispersion. For electrochemical examination, ethylene glycol (Merck), sodium perborate (Riedel) and KOH (Merck) were utilized as the fuel, the oxidant and the electrolyte, respectively. All the chemicals utilized have been of analytical grade (99.9 %) and have been utilized as-received.

Synthesis of Fe-Co-Ni nanoalloy catalysts: Ultrasonic-assisted chemical method of reduction was used to synthesize the biocarbon and carbon-supported Fe-Co-Ni nanoalloy catalysts.

The biocarbon from coconut shell was obtained by carbonization at 700 °C for 50 min under a nitrogen atmosphere. The Fe-Co-Ni nanoalloy catalysts supported by biocarbon were prepared by the $NaBH_4$ reduction process, utilizing cobalt(II) acetate tetrahydrate, iron(II) acetate and nickel(II) acetate tetrahydrate. In the preparation, biocarbon first allowed to disperse in isopropanol/water solution of 50/50v/v. The blend was made to homogenized under blending and then the metal forerunners $(CH_3COO)_2Co{\cdot}4H_2O$ (1.0 g, Merck), $Fe(CO_2CH_3)_2$, (1.0 g, Merck) and $Ni(OCOCH_3)_2{\cdot}4H_2O$ (1.5 g, Merck) were included to get metal stacking of 40 wt % and put into an ultrasonic shower for about 15 min. At that point, 10 mL of 0.15 M sodium borohydride in 0.1 mol/L potassium hydroxide was added in single portion under stirring at 25 °C. The ensuing solution of colloid was stirred for 15 more min and filtering and washing the solids were done with water. The precipitate was washed numerous times and after that dried at 80 °C for 2 h. Finally, the Fe-Co-Ni/BC (1:1:1) nanoalloy catalyst was dried under vacuum for 5 h. For a comparison, catalyst Fe-Co-Ni/C was moreover synthesized by the similar strategy as portrayed above.

Formation of working electrode: By mixing 1 mL of Nafion® solution (5 wt %) in 5 mL ultrapure millipore water and 50 mg powder of carbon-supported catalyst, the catalyst ink was prepared. Onto a freshly-polished glassy-carbon terminal, ultrasonically homogenized ink of about 3 µL was deposited. Then the solvent became dissipated at room temperature in an open air. The metal stacking on working terminal was found to be 0.28 mg_{metal}/cm^2.

Basic catalyst characterization: TEM was utilized to examine at the morphology of the scattered catalysts (Philips CM 12 TEM), mean particle size and the particle size distribution. The synthesized crystal structure of nanoalloy catalysts was characterized with the aid of powder XRD employing a Rigaku multiflex diffractometer (display RU-200 B) with Cu-Kα1 ($\lambda_{K\alpha1}$ = 1.5406 Å) radiation source running at room temperature, a tube voltage of 40 kV and a tube current was 40 mA. The 2θ precise regions were recorded between 20° and 90° at a scan rate of 5°/min. TEM is used to inspect the mean particle size. The crystallite size is affirmed from XRD pattern by utilizing Scherrer's formula [15]. In order to calculate the crystallite size and grid parameter of iron, Fe (2 2 0) diffraction peak was chosen. EDX analyzer chose the atomic ratio of the catalysts, which was facilitates with the TEM analyzer.

Electrochemical estimations and preparation of electrode All the electrochemical estimations were carried out by an electrochemical workstation (CH Instruments, USA - CHI-6650) in a standard three-electrode cell assembly consists of the Pt wire as a counter terminal, glassy-carbon disk as a working electrode and Ag/AgCl as a reference terminal. CO-stripping voltammetry in 1 M KOH electrolyte solution was used to calculate the electrochemical active surface area (ECASA) of the Fe-Co-Ni/BC and Fe-Co-Ni/C.

Adsorption of CO was found to pick up at 0.1 V *vs*. Ag/AgCl in a CO saturated solution for 10 min and in order to remove CO at the surface, the electrolyte was wiped clean with nitrogen for 10 min.

The electrochemical activity of oxidation of ethylene glycol response was determined by means of CV at a scan rate of 50 mV/s in a half cell at room temperature in a 1 M ethylene glycol and 1 M KOH solution. All potentials in this manuscript had been scaled towards Ag/AgCl.

RESULTS AND DISCUSSION

X-ray diffraction (XRD): The structural information of the catalyst was attained by XRD examinations. The XRD patterns of the prepared Fe-Co-Ni/BC and Fe-Co-Ni/C catalysts were shown in Fig. 1. The primary wide peak located at 20-30° within the XRD patterns is inferable to the carbon (0 0 2) plane. The 2θ of (2 2 0) peak for Fe-Co-Ni showed up a better angle shift than the characteristics of face-centered cubic (fcc) crystalline Fe. The 2θ values of Fe of 40°, 46°, 81° and 67° were recorded with planes (1 1 1), (2 0 0), (3 1 1) and (2 2 0) individually, demonstrating lattice contraction and alloy formations. These come about moreover showed that the Fe nanoparticles may well be homogenously alloyed with Co and Ni. The fcc grid parameters from the angular position of the (2 2 0) crests were assessed, which reflect arrangement of homogenous alloy particles. The obtained lattice parameters for the Fe-Co-Ni/BC (0.3890 nm) catalysts are smaller than those for Fe-Co-Ni/C (0.3903 nm). It is illustrated that decrease in grid parameters of alloy catalysts comes about from dynamic increment in the incorporation of Ni and Co into the alloyed state. The difference of lattice parameters and the shift of (2 2 0) plane illustrate interactions between Co-Ni and Fe. Using Scherrer's equation, the normal crystallite size was calculated. Table-1 lists crystallite size of the catalysts and lattice para-meters obtained from the XRD patterns.

TABLE-1
CHARACTERIZATION PARAMETERS FOR THE Fe–Co–Ni/BC AND Fe–Co–Ni/C NANOALLOY CATALYSTS

Electrocatalysts		(2 2 0) Diffraction peak position (2θ°)	Lattice parameter (nm)	Average crystallite size from XRD (nm)	Average particle size from TEM (nm)
Nominal	Experimental				
Fe–Co–Ni/BC	Fe–Co–Ni/BC	68.01	0.3890	3.4	2.9
Fe–Co–Ni/C	Fe–Co–Ni/C	67.84	0.3903	3.7	3.5

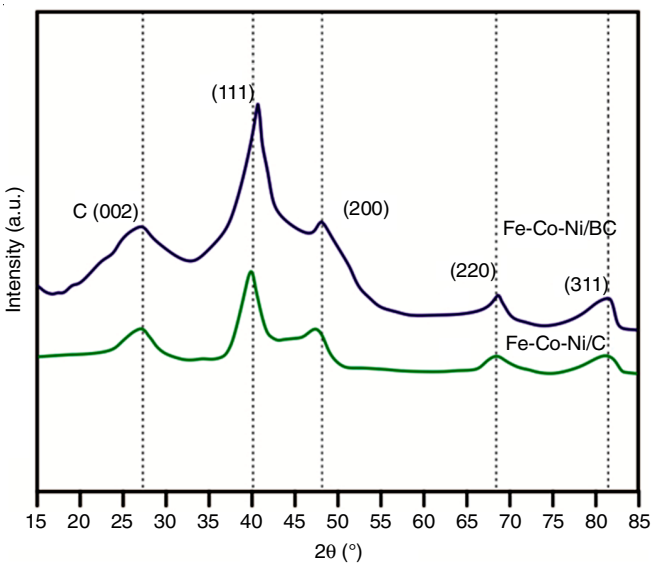

Fig. 1. XRD patterns of Fe-Co-Ni/BC and Fe-Co-Ni/C nanoalloy catalysts

Transmission electron microscopy (TEM): TEM images and the particle size dispersions of Fe-Co-Ni/BC as well as Fe-Co-Ni/C catalyst were shown in Fig. 2. As shown in Fig. 2, Fe-Co-Ni nanoparticles were consistently scattered on carbon. On the other hand, a few agglomerates were shaped on biocarbon support, which causes wide particle size dispersion. These results were in agreement with the XRD results, demonstrating that the size of the Fe-Co-Ni nanoparticles deposited was delicate to the structure of the biocarbon and it is seen that Fe-Co-Ni/BC is the foremost proficient catalyst than Fe-Co-Ni/C. The great scattering of Fe-Co-Ni/BC may be ascribed to better adsorbability of biocarbon determined from its high surface area. The catalysts particle size distribution is reported in Table-1, which was in agreement with TEM images. The mean particle size found by TEM picture and XRD investigation were comparative.

EDX analysis: EDX investigation was performed to test the presence of metallic particles. The prepared catalysts had

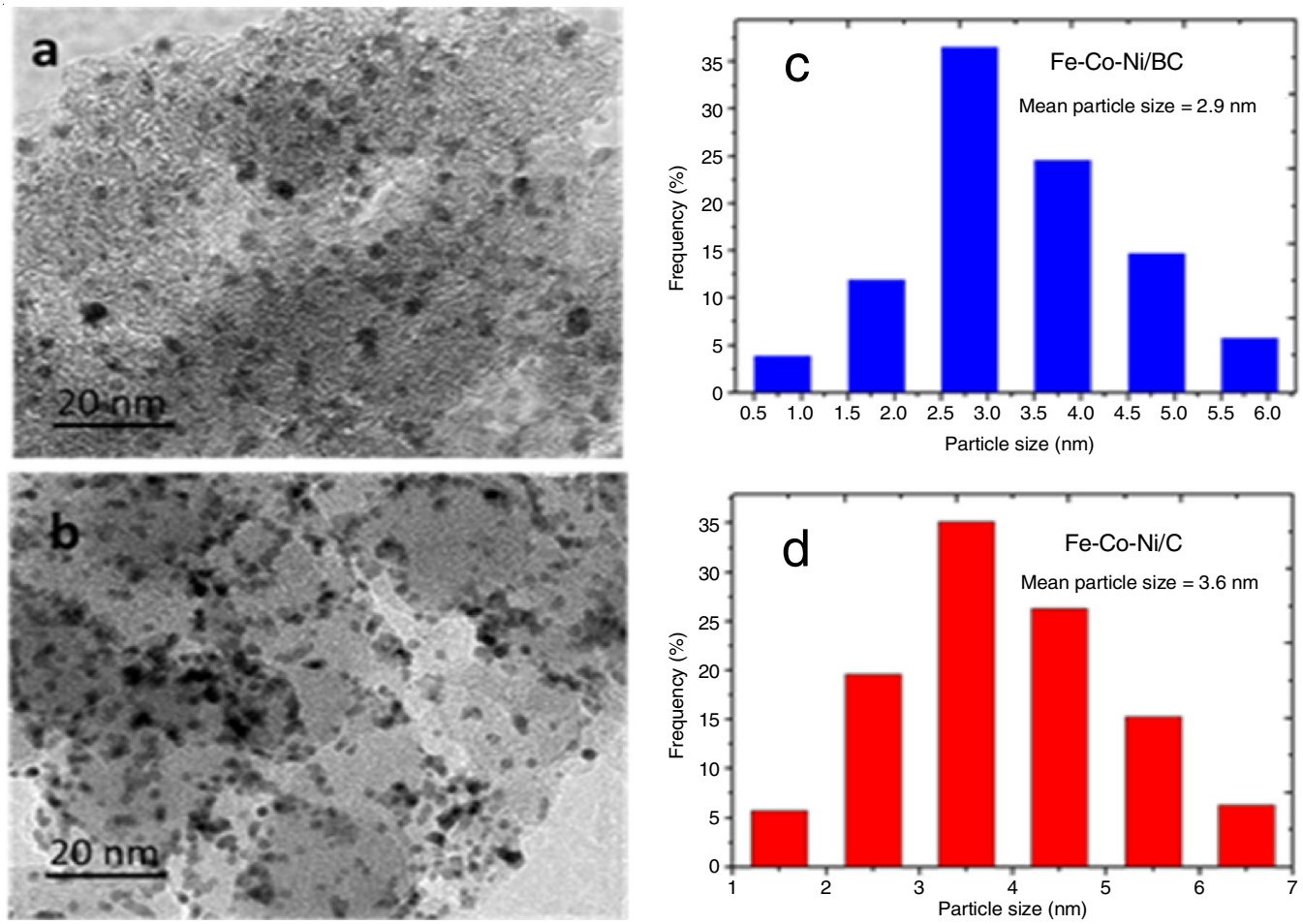

Fig. 2. TEM images and histograms of (a, c) Fe–Co–Ni/BC and (b, d) Fe–Co–Ni/C nanoalloy catalysts

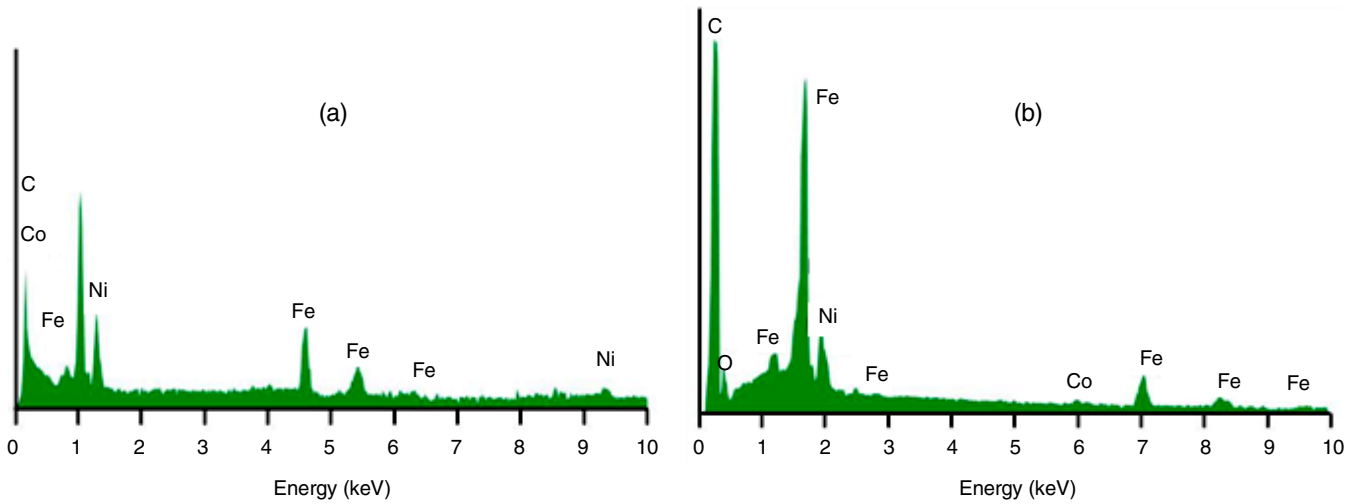

Fig. 3. EDX spectra of (a) Fe–Co–Ni/BC and (b) Fe–Co–Ni/C nanoalloy catalysts

specified components with a few variations in composition. The EDX investigations of the Fe-Co-Ni/BC and Fe-Co-Ni/C catalysts were shown in Fig. 3a and b. The Fe and Co–Ni signals found on all the figures show the effective deposition of these atoms on both biocarbon and carbon supports. The results of EDX examination assist affirm that the Fe:Co:Ni atomic ratio are closely 1:1:1, which was in understanding with the concentration proportion within the antecedent arrangements and is conceded to be the foremost active composition for the ethylene glycol electro-oxidation reaction.

Cyclic voltammetry (CV): The electrocatalytic activity of ethylene glycol oxidation on BC-supported Fe-Co-Ni nanoparticles was characterized by CV and compared with Fe-Co-Ni/C with and without ethylene glycol in an electrolyte of 1 M KOH at 50 mV/s. The voltammograms of each sample got to be comparable and steady after completion of tenth cycle. Fig. 4 shows the final voltammograms from the tenth cycle. The Fe-Co-Ni nanoparticles efficiencies were in comparison

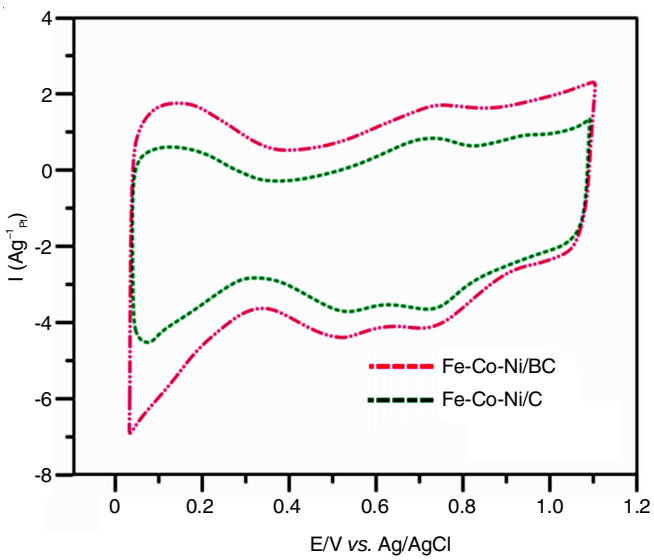

Fig. 4. Cyclic voltammetry of Fe-Co-Ni/BC and Fe-Co-Ni/C nanoalloy catalysts in 1 M KOH at room temperature with a scan rate of 50 mV/s

with oxidation peak current density, oxidation potential and the proportion of the forward peak to the reverse peak current density; this information were tabulated in Table-3.

Fig. 4 shows the CV of Fe-Co-Ni/C as well as Fe-Co-Ni/BC electrocatalysts deposited onto glassy-carbon electrode without ethylene glycol. Normal hydrogen adsorption/hydrogen desorption peaks were noted within potential extend from –0.2 to 0.1 V (*vs.* Ag/AgCl). Hence, range of hydrogen adsorption or hydrogen desorption on CV bends can be utilized to calculate the ECASA of Fe catalysts. It is known that the ECASA reveals the accessible number of active sites on catalyst surface for electrochemical reactions. It decides the effective transport routes for electrons on electrode surface; in this manner, bigger the ECASA, higher the electrocatalytic movement for ethylene glycol oxidation responses (MOR) [16]. The ECASA of Fe-Co-Ni/C and Fe-Co-Ni/BC nanoalloy catalysts can be calculated concurring to eqns. 1 and 2 [17]:

$$S_{ECASA/H}\left(\frac{m^2}{g}\right)=\frac{Q_H\left(\frac{\mu C}{cm^2}\right)}{210\left(\frac{\mu C}{cm^2}\right)\times 0.77\times[Pt]} \quad (1)$$

$$S_{ECASA/CO}\left(\frac{m^2}{g}\right)=\frac{Q_{CO}\left(\frac{\mu C}{cm^2}\right)}{420\left(\frac{\mu C}{cm^2}\right)\times[Pt]} \quad (2)$$

where Q_H the charges corresponding to desorption of hydrogen on the Fe surface, [Fe] (mg/cm^2) iron stacking on the electrode surface; the charge needed to oxidize a monolayer of hydrogen on the Fe surface is 210 μC/cm and the hydrogen monolayer coverage is 0.77 [18]. The ECASA of different catalysts were reported based on eqn. 1 and were recorded in Table-2. The calculated ECASA of Fe-Co-Ni/BC (67 m^2/g) were higher than that of Fe-Co-Ni/C (37 m^2/g). Due to the smaller size and uniform dissemination of Fe-Co-Ni nanoparticles, electrochemically active surface zone of Fe-Co-Ni/BC is the most noteworthy.

TABLE-2
COMPARISON OF HYDROGEN DESORPTION CHARGE AND CARBON MONOXIDE DESORPTION CHARGE WITH ITS ECASA AND ELECTRODE ROUGHNESS

Catalyst	Q_H/μ_C	$Q_{CO}/\mu C$	Electrode real surface area (cm^2)	ECASA/H (m^2/g)[a]	ECASA/CO (m^2/g)[a]	Roughness
Fe–Co–Ni/BC	541.6	1491	3.5	67	71	99.4
Fe–Co–Ni/C	299.1	882	2.1	37	42	58.8

[a]The ECASA area ($S_{ECASA/H}$ and $S_{ECASA/CO}$) were calculated from eqns. 1 and 2.

Fig. 5 shows Fe-Co-Ni/C and Fe-Co-Ni/BC catalysts' CO-stripping voltammograms were recorded in 1 M KOH between 0.05 and 0.9 V against Ag/AgCl at a scan rate of 50 mV/s. A CO_{ads} oxidation crest is noted at 0.26 and 0.32 V against Ag/AgCl for Fe-Co-Ni/C and Fe-Co-Ni/BC, separately. For the Fe-Co-Ni/BC nanoparticles, a cathodic move of at least 100 mV due to CO oxidation was happened, compared with Fe-Co-Ni/C. The crest positions within the voltammograms of Fe-Co-Ni/C and Fe-Co-Ni/BC nanoparticles are comparative, but the crests of BC-supported nanoparticles are higher symmetric than those of carbon-supported substrates. The higher symmetry of Fe-Co-Ni/BC of oxidation crest in voltammograms recommends that successful, strong electronic interactions take place between the Fe-Co-Ni nanoparticles and the biocarbon.

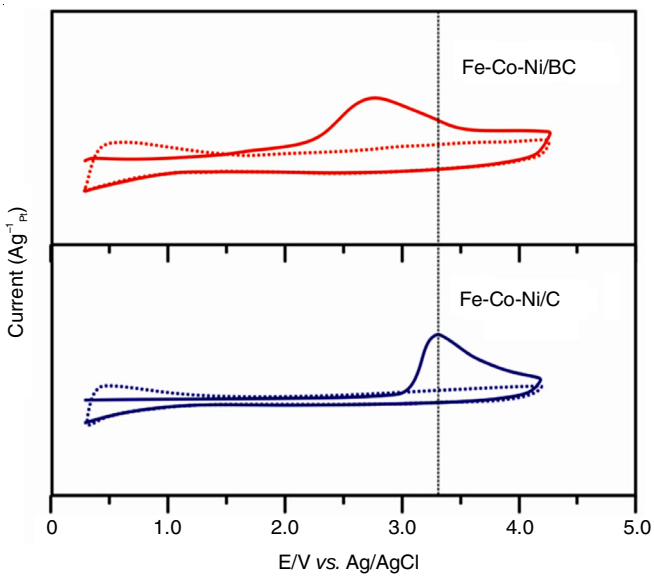

Fig. 5. CO stripping voltammetry of Fe-Co-Ni/BC and Fe-Co-Ni/C nanoalloy catalysts in 1 M KOH at room temperature with a scan rate of 50 mV/s

Fig. 6 shows the CVs of ethylene glycol electro-oxidation catalyzed by Fe-Co-Ni/C as well as Fe-Co-Ni/BC catalysts in 1 M ethylene glycol and 1 M KOH solution at room temperature. In carbon as well as BC-supported Fe-Co-Ni electrodes, two oxidation crests can be noticed on the forward scan and a single crest can be noted on the reverse scan towards oxidation-reduction responses. The crest within the forward scan is related with the oxidation of ethylene glycol and the crest in the reverse scan is related to the carbonaceous intermediate products due to oxidation formed from deficient ethylene glycol oxidation. The proportion of forward crest current (I_F) to backward crest

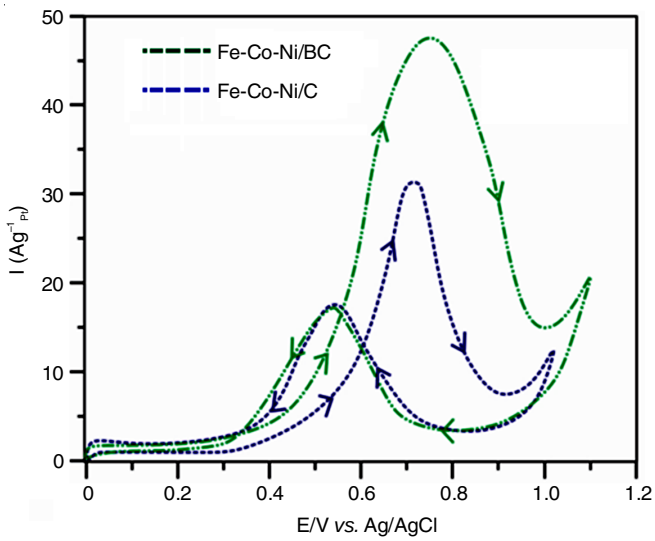

Fig. 6. Cyclic voltammetry of Fe-Co-Ni/BC and Fe-Co-Ni/C nanoalloy catalysts in 1 M KOH and 1 M ethylene glycol at room temperature with a scan rate of 50 mV/s

current (I_B) is utilized to determine the resistance of catalysts to aggregation of intermediate carbonaceous species [8,19-22]. A higher I_F/I_B value shows higher tolerance of intermediate carbon species. The data obtained from Fig. 6 were also listed in Table-3.

TABLE-3
CV RESULTS OF Fe–Co–Ni/BC AND Fe–Co–Ni/C NANOALLOY CATALYSTS AT ROOM TEMPERATURE

Catalysts	Forward anodic peak (I_F) (mA/cm^2)	Backward anodic peak (I_B) (mA/cm^2)	I_F/I_B ratio
Fe–Co–Ni/BC	48.7	18.4	2.6
Fe–Co–Ni/C	32.6	18.5	1.7

The nanoalloy catalysts in this study, the Fe-Co-Ni/BC catalysts shown a esteem I_F/I_B value (2.6) than the Fe-Co-Ni/C (1.7), showing the much more complete ethylene glycol oxidation in the forward scan and also the effective evacuation of harming CO-like species from the catalysts surface. The high electrocatalytic activity of Fe-Co-Ni/BC concurs well with the little particle size and the catalyst excessive electrochemically active surface area. As shown in Fig. 6, the onset potentials of Fe-Co-Ni/BC for ethylene glycol electrooxidation were noted at 0.25 V, whereas the onset potentials of Fe-Co-Ni/C were at 0.32 V *vs.* Ag/AgCl, individually. In addition, the results not only demonstrate that the onset potentials move to negative direction on Fe-Co-Ni/BC compared with Fe-Co-Ni/C, but also reveal that the peak current densities become

much bigger, demonstrating ethylene glycol electro-oxidation is more dynamic on BC-based catalysts than that on carbon support catalysts.

The upgraded activity of Fe-Co-Ni/BC catalyst can be clarified as follows: biocarbons have plenteous and consistently dispersed mesopores, which is advantageous for the uniform scattering of Fe-Co-Ni particles. In expansion, the mesopores of biocarbon have special 3D interconnection, which is in favour of the productive dissemination of fuel (ethylene glycol) and reaction products. In contrast, the carbon support appears to be a nonporous material. Fe-Co-Ni particles were scattered arbitrarily on the surface of carbon nanoparticles and thus were inclined to agglomerate. Also, so-called nanopores in carbon were from an arbitrary stack of carbon particles and their interconnection ought to not be as great as that of mesopores in biocarbons. As a result of the above contrast of pore structure, the Fe-Co-Ni/BC catalyst has higher capacity to exert the catalytic activity of Fe-Co-Ni particles and in this way has better electrochemical exhibitions than the Fe-Co-Ni/C. The CV consequences of synthesized electrocatalysts including positive peak potentials, the onset potentials and the corresponding peak current densities of MOR were tabulated in Table-4.

TABLE-4
POSITIVE PEAK POTENTIAL AND PEAK CURRENT DENSITY OF Fe–Co–Ni/C AND Fe–Co–Ni/BC NANOALLOY CATALYSTS AT ROOM TEMPERATURE

Catalyst	Onset potential (V)	Scan rate 50 mV/s	
		Positive peak potential (V *vs.* Ag/AgCl)	Peak current density (mA/cm^2)
Fe–Co–Ni/BC	0.26	0.71	48.7
Fe–Co–Ni/C	0.32	0.74	32.6

Chronoamperometry: The electrocatalyst performances of Fe-Co-Ni/C and Fe-Co-Ni/BC for oxidation of ethylene glycol were examined for 2 h by chronoamperometry at 0.7 V *vs*. Ag/AgCl to examine both the electrocatalytic activity of the catalysts and poisoining of active surface under persistent operation conditions. Chronoamperograms obtained for the distinctive electrocatalysts and its current densities were normalized by Fe mass were shown in Fig. 7. Amid primary 5 min, a sharp decrease within the current density and followed by relative stabilization turned into noted. This happens since active sites were at first free from the adsorbed ethylene glycol/oxidized ethylene glycol molecules. Fe-Co-Ni/C gave rise to extremely quick rates of poisoining of catalytic sites, resulting in an awfully low activity. In any case, the BC-supported Fe-Co-Ni catalyst had a great capacity to overcome catalyst poisoining, thus furnishing a high current density. The BC-supported (Fe-Co-Ni/BC) electrocatalysts illustrated higher current than the C-supported (Fe-Co-Ni/C) electrocatalysts. Higher current obtained for the Fe-Co-Ni/BC may be because of mesopores structure and high surface area of biocarbon.

Single cell performance: The microfluidic design of laminar flow-based membraneless fuel cells overcomes the water administration problems and fuel hybrid that plague membrane-based fuel cells (PEMFC, DMFC) and empowers auto-

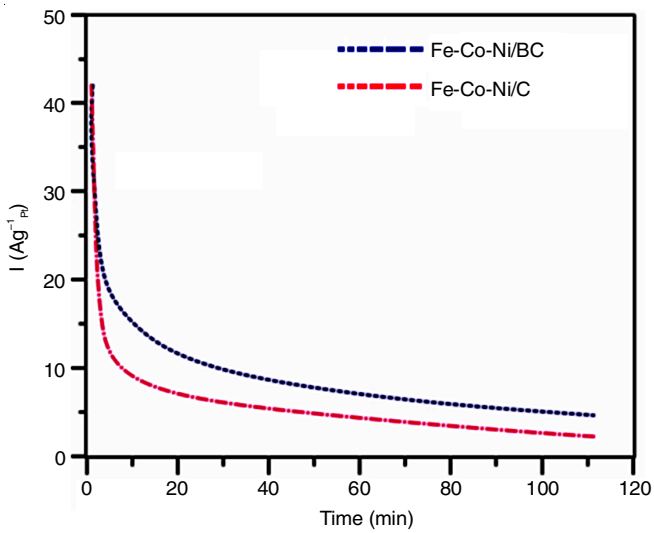

Fig. 7. Chronoamperometry of Fe-Co-Ni/BC and Fe-Co-Ni/C nanoalloy catalysts with a scan rate of 50 mV/s

nomous stream characteristics control (*i.e.* composition and flow-rate). Here, in terms of power density it is targeted on maximizing cell execution by fitting different structural traits and catalytic activity of biocarbon and carbon supported Fe-Co-Ni catalysts. A single membraneless ethylene glycol fuel cell (MLEGFC) was tried utilizing the Fe-Co-Ni/C and Fe-Co-Ni/BC catalysts as anode. Power densities and polarization curves are shown in Fig. 8. The catalyst loadings at both electrodes are 0.28 mg/cm^2 and Fe/BC was utilized as cathode catalyst. The OCVs of Fe-Co-Ni/BC are higher than that of Fe-Co-Ni/C and the arrangement of OCV was precisely the same as the onset potentials. In spite of the fact, that the distinction between Fe-Co-Ni/BC and Fe-Co-Ni/C is moderately little within the low-current-density region, the critical support effect of biocarbon gets to be larger as the current density increments. Moreover, a fast initial fall in cell voltage was occurred for both catalysts, which was because of the moderate beginning of electrooxidation reaction of ethylene glycol at the electrode surface. After a beginning drop of 50 mV, alter in incline of polarization bend was seen for Fe-Co-Ni/BC faded and begun drawing greater current. This occasion can be credited

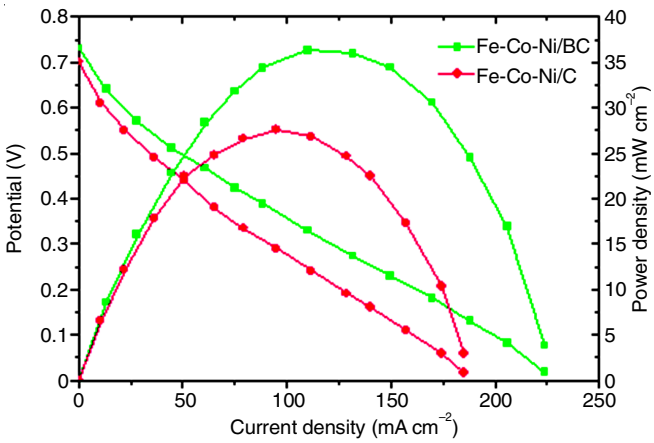

Fig. 8. Polarization and power density curves of Fe-Co-Ni/BC and Fe-Co-Ni/C nanoalloy catalysts at room temperature

to the more compelling catalytic ability of Fe-Co-Ni/BC, once the ethylene glycol oxidation reaction is initiated. The results of MLEGFC receiving to C and BC-supported catalysts were tabulated in Table-5. On basis of drawn peak power density using single cell, Fe-Co-Ni/BC is the finest anode catalyst with 36.3 mW/cm^2 as crest power density.

TABLE-5
PERFORMANCE OF SINGLE FUEL CELL TESTS USING Fe–Co–Ni/BC AND Fe–Co–Ni/C NANOALLOY CATALYSTS

Anode catalysts	Open circuit voltage (V)	Maximum power density (mW/cm^2)	Maximum current density (mA/cm^2)
Fe–Co–Ni/BC	0.73	36.3	224
Fe–Co–Ni/C	0.70	30.2	185

Conclusion

Carbon supported Fe-Co-Ni nanoalloy catalysts were synthesized by chemical reduction method and their electrocatalytic activity for oxidation of ethylene glycol in membraneless fuel cell was well explored and compared with Fe-Co-Ni/BC. The crystallite measure, grid parameter, composition and particle size of metals within the catalysts were determined by XRD, EDX and TEM strategies, individually. The XRD designs of the prepared Fe-Co-Ni/C and Fe-Co-Ni/BC nanoalloy catalysts revealed the fcc crystalline characteristics of Fe at 2θ values of 40°, 47°, 67° and 81° ordered with planes (1 1 1), (2 0 0), (2 2 0) and (3 1 1), individually. The diminish within the grid parameters of the Fe alloy catalyst reflects the dynamic increment in the incorporation of Co-Ni into the alloyed state. TEM images have diameter of 2.9-3.5 nm with spherical shape and were consistently scattered on the surface of biocarbons. Cyclic voltammetric results showed that the Fe-Co-Ni/BC was more dynamic in ethylene glycol electro-oxidation than in Fe-Co-Ni/C. CA results showed that the BC-supported Fe-Co-Ni nanoalloy catalyst gave higher current than the carbon-supported Fe-Co-Ni catalysts. The power density gotten for Fe-Co-Ni/C (30.2 mW/cm^2) was lower than that of Fe-Co-Ni/BC (36.3 mW/cm^2) utilizing 0.1 M sodium perborate + 1 M KOH as cathode nourish and 1 M ethylene glycol + 1 M KOH as anode support. The higher catalytic execution of Fe-Co-Ni/BC may be ascribed to the mesopores of biocarbon advancing the mass transportation of ethylene glycol in catalyst layer. This concludes that both the surface chemistry and the morphology of the support have an vital effect on the scattering, particle size and activity of Fe-Co-Ni nanoalloy catalysts. Hence, the BC-supported Fe-Co-Ni nanoalloy catalysts are anticipated to be broadly utilized in electrocatalytic energy-conversion applications.

CONFLICT OF INTEREST

The authors declare that there is no conflict of interests regarding the publication of this article.

REFERENCES

1. J. Chen, M. Wang, B. Liu, Z. Fan, K. Cui and Y. Kuang, *J. Phys. Chem. B*, **110**, 11775 (2006); https://doi.org/10.1021/jp061045a
2. A. Halder, S. Sharma, M.S. Hegde and N. Ravishankar, *J. Phys. Chem. C*, **113**, 1466 (2009); https://doi.org/10.1021/jp8072574
3. N. Jha, M.M.L. Mohana Reddy, M. Shaijumon, N. Rajalakshmi and S. Ramaprabhu, *Int. J. Hydrogen Energy*, **33**, 427 (2008); https://doi.org/10.1016/j.ijhydene.2007.07.064
4. J. Kua and W.A. Goddard III, *J. Am. Chem. Soc.*, **121**, 10928 (1999); https://doi.org/10.1021/ja9844074
5. Y. Lin, X. Cui, C. Yen and C.M. Wai, *J. Phys. Chem. B*, **109**, 14410 (2005); https://doi.org/10.1021/jp0514675
6. M. Priya, S. Kiruthika and B. Muthukumaran, *J. Mater. Environ. Sci.*, **8**, 410 (2017).
7. S. Chaudhary, P. Sharma, P. Chauhan, R. Kumar and A. Umar, *Int. J. Environ. Sci. Technol.*, **16**, 5331 (2019); https://doi.org/10.1007/s13762-019-02253-2
8. Z. Liu, X.Y. Ling, X. Su and J.Y. Lee, *J. Phys. Chem. B*, **108**, 8234 (2004); https://doi.org/10.1021/jp049422b
9. M. Priya and B. Muthukumaran, *J. Indian Chem. Soc.*, **96**, 103 (2019).
10. T.D. Burchell, Carbon Materials for Advanced Technologies, Elsevier Science: Oxford (1999).
11. K. Kinoshita, Carbon: Electrochemical and Physicochemical Properties, John Wiley & Sons: New York (1998).
12. J. Ribeiro, D. M. dos Anjos, K. B. Kokoh, C. Countanceau, J. M. Leger, P. Olivi, A. R. de Andrade, and G. Tremiliosi-Filho, *Electrochim. Acta*, **52**, 6997 (2007); https://doi.org/10.1016/j.electacta.2007.05.017
13. Z.B. Wang, P.J. Zuo and G.P. Yin, *J. Alloys Compd.*, **479**, 395 (2009); https://doi.org/10.1016/j.jallcom.2008.12.061
14. Z. Wang, G. Yin, J. Zhang, Y. Sun and P. Shi, *J. Power Sources*, **160**, 37 (2006); https://doi.org/10.1016/j.jpowsour.2006.01.021
15. V. Radmilovic, H.A. Gasteiger Jr. and P.N. Ross, *J. Catal.*, **154**, 98 (1995); https://doi.org/10.1006/jcat.1995.1151
16. H.P. Cong, X.C. Ren and S.H. Yu, *ChemCatChem*, **4**, 1555 (2012); https://doi.org/10.1002/cctc.201200403
17. A. Arun, M. Gowdhamamoorthi, K. Ponmani, S. Kiruthika and B. Muthukumaran, *RSC Adv.*, **5**, 49643 (2015); https://doi.org/10.1039/C5RA04958J
18. T. Biegler, D.A.J. Rand and R. Woods, *J. Electroanal. Chem.*, **29**, 269 (1971); https://doi.org/10.1016/S0022-0728(71)80089-X
19. T.C. Deivaraj and J.Y. Lee, *J. Power Sources*, **142**, 43 (2005); https://doi.org/10.1016/j.jpowsour.2004.10.010
20. R. Mancharan and J.B. Goodenough, *J. Mater. Chem.*, **2**, 875 (1992); https://doi.org/10.1039/jm9920200875
21. T. Maiyalagan, *J. Solid State Electrochem.*, **13**, 1561 (2009); https://doi.org/10.1007/s10008-008-0730-0
22. Y. Mu, H. Liang, J. Hu, L. Jiang and L. Wan, *J. Phys. Chem. B*, **109**, 22212 (2005); https://doi.org/10.1021/jp0555448